Research Square

Preprints are preliminary reports that have not undergone peer review.
They should not be considered conclusive, used to inform clinical practice,
or referenced by the media as validated information.

Machine learning-based regression and multi-objective optimization of thermo-hydraulic performance in a tubular heat exchanger with co- and counter-arranged V-winglet twisted tape inserts

Bipin Kumar
Dehradun Institute of Technology University
Himani Sharma
Dehradun Institute of Technology University
Anil Kumar Patil
akpt1711978@gmail.com

Dehradun Institute of Technology University
Manoj Kumar
Sankalchand Patel University

Research Article

Keywords: Machine learning, Twist ratio, V-winglet twisted tape, Entropy generation number

Posted Date: August 25th, 2026

DOI: https://doi.org/10.21203/rs.3.rs-10239355/v1

License: This work is licensed under a Creative Commons Attribution 4.0 International License.
Read Full License

Additional Declarations: No competing interests reported.

Machine learning-based regression and multi-objective optimization of thermo-hydraulic performance in a tubular heat exchanger with co-and counter-arranged V-winglet twisted tape inserts

BIPIN KUMAR[1#], HIMANI SHARMA[2$], ANIL KUMAR PATIL[1*], MANOJ KUMAR[3^]
[1] Department of Mechanical Engineering, DIT University, Dehradun 248009, India.
[2] Department of Computer Science Engineering, DIT University, Dehradun 248009, India.
[3]Department of Mechanical Engineering, Faculty of Engineering, Sankalchand Patel University, Vishnagar, Gujarat, Mehsana, 384315, India.
[3]Department of Mechanical Engineering, Graphic Era Deemed University, Dehradun 248002, Uttarakhand, India.
[#]bipinydv@gmail.com, [$]himani.sharma@dituniversity.edu.in, [*]akpt1711978@gmail.com, dr.anilpatil@dituniversity.edu.in, [^]kmanoj1947@gmail.com, mksmech_spce@spu.ac.in

Abstract

V-winglet double perforated twisted tape (DPTT) turbulators configured in co-swirl (CO) and counter-swirl (COT) orientations are widely employed for heat transfer enhancement in heat exchangers. However, studies that lead to systematic optimisation remain limited, particularly in exergetic performance, advanced exergy analysis, and the integration of machine learning (ML) techniques. The present study develops a data-driven framework for predicting and optimizing the thermo-hydraulic performance of double perforated twisted tape configurations by integrating multi-model machine learning, explainable artificial intelligence (XAI), and multi-objective optimization. The dataset includes key operational and geometric parameters, namely Reynolds number (Re) ranging from 10,400 to 22,800 and twist ratio (y) ranging from 2 to 6, along with corresponding outputs: Nusselt number (Nu), friction factor (f), thermal performance factor (η), and entropy generation number (N_s). Machine learning models (MLR, RF, XGBoost, LS-SVM, and ANN) were trained and evaluated to predict the Nu, f, η, and N_s. Model robustness and generalization were validated using parity plots, REC curves, and cross-validation. LS-SVM and XGBoost models showed high accuracy in predicting the key parameters. Multi-objective optimization using NSGA-II yielded Pareto-optimal solutions that balance heat transfer enhancement and frictional losses.

Keywords: Machine learning, Twist ratio, V-winglet twisted tape, Entropy generation number.

1. Introduction

Fast paced development of modern society exponentially rises the demand for energy, necessitating continuous improvements in energy conversion systems. Heat exchangers facilitate heat energy exchange between working fluids under varying operating conditions. Significant steps have been taken to improve their performance by reducing energy losses. Passive techniques of heat transfer enhancement are popular due to their simplicity, cost-effectiveness, and ease of implementation. Use of inserts such as perforated

plates, conical rings, vortex generators, spring inserts, and swirl flow devices enhance heat transfer by promoting fluid mixing and turbulence and thereby reviving the thermal boundary layer. In recent years, machine learning (ML) gains popularity due to its effectiveness in modelling and optimization of heat exchanger system. ML techniques such as artificial neural networks (ANN), support vector machines (SVM), and random forests (RF) accurately predict complex thermo-hydraulic behaviour across a wide range of operating conditions unlike conventional methods, which are time-intensive, costly, and limited in generalizability. Highly efficient heat exchanger systems can be designed using machine learning integrated performance prediction, design optimization, and energy efficiency enhancement.

2. Literature review and research objectives

Twisted tapes are widely used as tube inserts, transforming the axial tube flow into swirl flow by directing the flow along the twisted tape surface. Twist ratio appeared to be the most influential parameter of twisted tape, which significantly contributes in the enhancement of heat transfer rates [1- 4]. Twin twisted tapes have produced higher thermal enhancement than a single tape [5]. Moreover, double twisted tapes in counter-swirl orientation yielded higher enhancement compared to a co-swirl orientation of insert. Later, the concept of employing multiple twisted tapes was introduced to multiply the thermal enhancement by manifolds [6-9]. It is seen that the typical twisted tape dissipates considerable amount of energy to overcome frictional loss caused by greater contact surface area and swirl flow. Perforations in twisted tape were introduced to reduce the friction loss by way of minimizing surface friction and form drag [10]. It was discovered that higher perforation weakened the swirling effect and a low porosity helped in generating strong swirl intensity [11]. The double counter-swirl twisted tapes with perforations were also found beneficial to achieve higher thermo-hydraulic performance [12]. An introduction of V cut on the out edges of tape produced higher heat transfer enhancement than that of solid and perforated twisted tape [13]. Kumar et al. [14] conducted an experimental investigation using perforated twisted tape inserts with multiple V-shaped cuts. The minimum entropy generation rate was attained for the tube fitted with perforated twisted tape at a twist ratio of 3. Jayranaiwachiraa et al. [15] experimentally investigated the thermo-hydraulic characteristics and entropy generation behaviour of a louvered corner-curved V-baffle tape (LCVT). The highest thermal energy performance factor (TEF) was achieved under optimal operating conditions; however, the minimum entropy generation corresponded to comparatively lower TEF values. Heeraman et al. [16] demonstrated in a study that the dimpled twisted tape inserts significantly improved the heat transfer rate compared to both plain twisted tape and a smooth tube. Mertaslan et al. [17] carried out an experimental study to evaluate the combined effect of hybrid nanofluids and barrel-type wire inserts, yielding a higher second-law efficiency. Celik et al. [18] investigated the effects of Reynolds number and tape geometry on entropy generation,

exergy destruction, second-law efficiency, and NTU. Lasso and Elastic Net models exhibited higher predictive accuracy ($R^2 \approx 0.98$) compared to the MLR model. Khan et al. [19] demonstrate that an artificial neural network (ANN) can accurately predict the thermal performance of heat exchangers with delta-wing tape inserts. It was observed that the ANN approach efficiently proposes a heat exchanger design for delivering optimal performance. Kunakote et al. [20] proposed an integrated machine learning (ML)-assisted metaheuristic (MH) framework for the optimization of corrugated tube (CT) heat exchangers. CFD simulations help analyze the effects of corrugation number, depth ratio, and pitch ratio, and integrated ML surrogate models predict the data accurately for optimization. Han et al. [21] optimized corrugated tubes with multi-channel twisted tape using RSM and NSGA-II models with a reasonable accuracy.

The perforated double twisted tape inserts with CO/COT configurations significantly improve heat transfer while reducing pressure drop losses. The presence of periodically arranged V-winglets along the edges of the twisted tape near the tube wall is thought to generate secondary fluid flows, enhancing turbulence and thereby increasing the heat transfer rate. Also, this study proposes a unified data-driven framework combining multi-model machine learning, explainable AI, and NSGA-II optimization to predict and enhance the thermo-hydraulic performance of twisted tape configurations. The flow parameter such as Reynolds number and tape geometry strongly influences the thermal and hydraulic performance depicted by Nu, f, η, N_s. The application of LS-SVM and XGBoost modelling predicts these parameters with high accuracy, while Pareto-optimal solutions balance heat transfer and frictional losses.

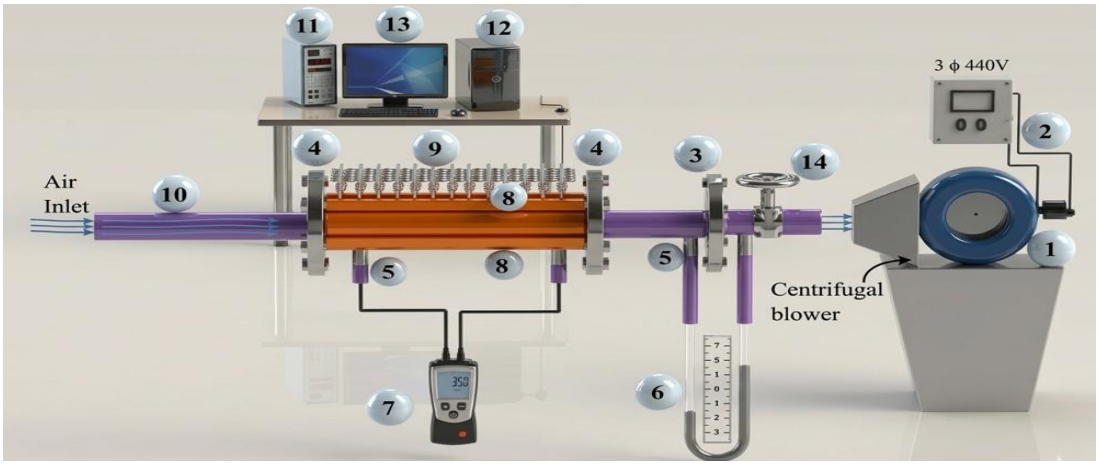
The present study aims to achieve the following objectives:

- Experimental data collection on a heat exchanger tube fitted with (DPTT) having V-winglet in (CO) and (COT) orientations by varying Re from 10400-22800.
- Thermal and hydraulic assessment of data to apprise different twisted tapes.
- To optimize the insert parameters based on entropy generation in the test section due to different geometries of twisted tape.
- To maximize heat transfer performance for minimal frictional losses and entropy generation, using NSGA-II-based multi-objective optimization.

3. Methodology

The experimental test setup has a 3 m long cylindrical tube of 0.032 m ID which is divided into inlet, test, and exit sections. A centrifugal blower of 2 HP rated power draws atmospheric air through the test section at different mass flow rates using a gate valve. The cylindrical tube receives heat energy from the heating

element uniformly wrapped around the outer tube surface. The test setup layout is shown in Figure 1. The test section has a composite layer of glass wool tape and insulating foam. The temperature of tube wall is measured at different axial locations using T-type thermocouples. The temperature of air at inlet and exit sections are also measured. A micro manometer is installed across the test section to record the pressure drop and a U-tube manometer is employed on upstream side of the blower to compute mass flow rate of air. The experimental data have been collected under steady state conditions during the test run for various mass flow rates of air in the range of 0.005 to 0.01 kg/s corresponding to the Reynolds number from 10400 to 22800. Various twisted tape geometries are shown in Figure 2. Aluminium is used to manufacture the twisted tapes, which has a thermal conductivity of 237 W/m-K [22]. Circular perforations of 6 mm diameter are created along the axis of tape at an interval of pitch length (p). The twist ratio (y = p/w) of tapes has been varied from 2 to 6 in three steps. The range of parameters is shown in Table 1.



(1) Air blower	(8) Test section
(2) 3-Phase Electric Switch	(9) T-type thermocouples
(3) Orifice	(10) Inlet section
(4) Flanges	(11) Data-logging system
(5) Manometer limbs	(12) CPU
(6) Manometer (U-tube)	(13) Monitor
(7) Manometer (Digital)	(14) Flow control valve

Figure 1: Schematic representation of the experimental setup.

The geometrical configurations of the twisted tape inserts are presented in Figure 2. Axially aligned circular perforations of 6 mm diameter are incorporated at a specified pitch (P). V-shaped winglets are integrated along the longitudinal edges of the DPTT-CO and DPTT-COT configurations. The winglet depth ratio (d_c/W) is defined as the ratio of the cut depth (d_c) to the tape width (W), whereas the winglet width ratio (w_c/W) is expressed as the ratio of the cut width (w_c) to the tape width (W).

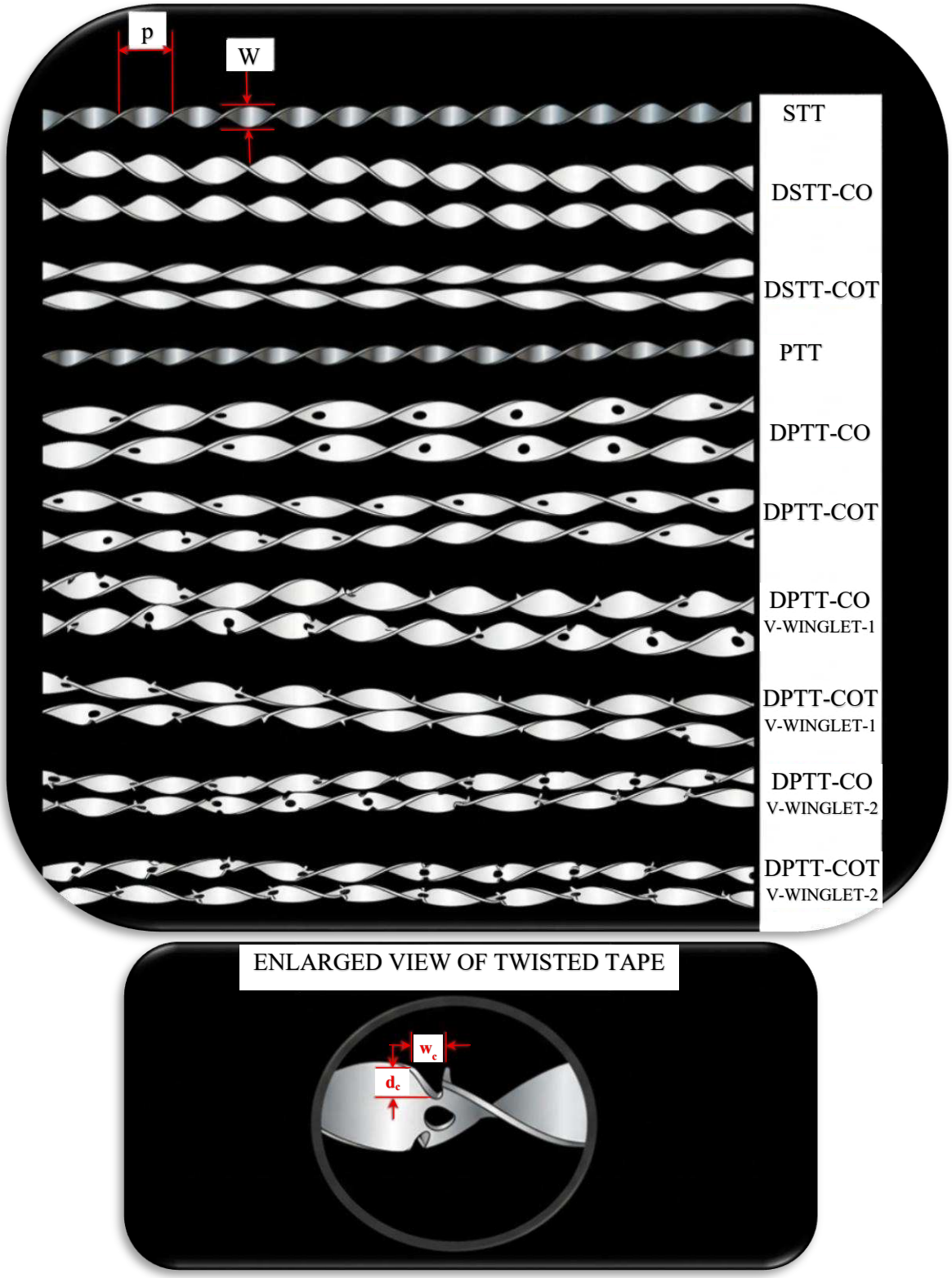


Figure 2: The structural configuration of twisted tape inserts.

The test run initiates with supplying a pre-defined air flow rate. The heating element is put on to maintain uniform heat flux on test section. The temperature and pressure are monitored till the system attains a steady state. Similar tests were conducted at different mass flow rate of air.

Table 1 Parametric range

S.No.	Parameters	Range
1.	Twist ratio (y: p/W)	2, 4, and 6
2.	Winglet depth ratio (d_c/W)	0.2
3.	Winglet width ratio (w_c/W)	0.2
4.	Porosity ratio (R_P)	0.045
5.	Reynolds Number (Re)	10,400 to 22,800

4. Experimental data processing and analysis

Test runs generate a pool of measurable data under steady state conditions for each type of twisted tape. The mathematical analysis of raw data leads to obtain the dimensionless parameters such as Nu, Re, and f.

The analysis has been carried out as given under:

The energy balance helps to find the convective coefficient of heat transfer (h) as,

$$\mathrm{h} = \mathrm{Q}\mathrm{A}_s\Delta T_m \tag{1}$$

where LMTD (ΔT_m) is:

$$\Delta T_m = \frac{(\Delta T_i - \Delta T_o)}{\ln\left(\frac{\Delta T_i}{\Delta T_o}\right)} \tag{2}$$

where temperature excess of tube wall at inlet and exit section relative to air stream is represented as ΔT_i and ΔT_o, respectively.

The Nusselt number (*Nu*) is:

$$Nu = hD_i/k \tag{3}$$

where D_i and k represent the tube ID and thermal conductivity of air, respectively.

The Reynolds number (*Re*) is:

$$Re = \frac{\rho\, v\, D_i}{\mu} \tag{4}$$

where ρ is air density, v is air velocity, and μ is the dynamic viscosity of air.

The friction factor (f) is:

$$f = \frac{2\, \Delta p\, D_i}{\rho L v^2} \tag{5}$$

where Δp is the pressure drop.

The thermal performance factor (η) is defined as,

$$\eta = \frac{(Nu/Nu_s)}{(f/f_s)^{1/3}} \tag{6}$$

The uncertainties in parameters are reported in Table 2. The performance of a heat exchanger is fundamentally governed by the rate of heat transfer and the minimization of entropy generation. Any augmentation in heat transfer is intrinsically associated with exergy destruction arising from irreversible effects during steady-flow operation; consequently, entropy generation is quantified using the following thermodynamic relations [23].

$$\mathrm{N_s} = \dot{\mathrm{S}}_{\mathrm{g,r}}/\dot{\mathrm{S}}_{\mathrm{g,s}} \tag{7}$$

Entropy generation number (N_s) less than unity is considered desirable for keeping the irreversibility within the system under a safe limit.

The uncertainties in the experimentally determined Reynolds number (Re), Nusselt number (Nu), and friction factor (f) were found to be 2.01%, 2.91%, and 3.65%, respectively. The validation plot for Nu and f is shown in Figure 3 where the mean absolute deviation in Nu and f are obtained as 4.92% and 3.92%, respectively.

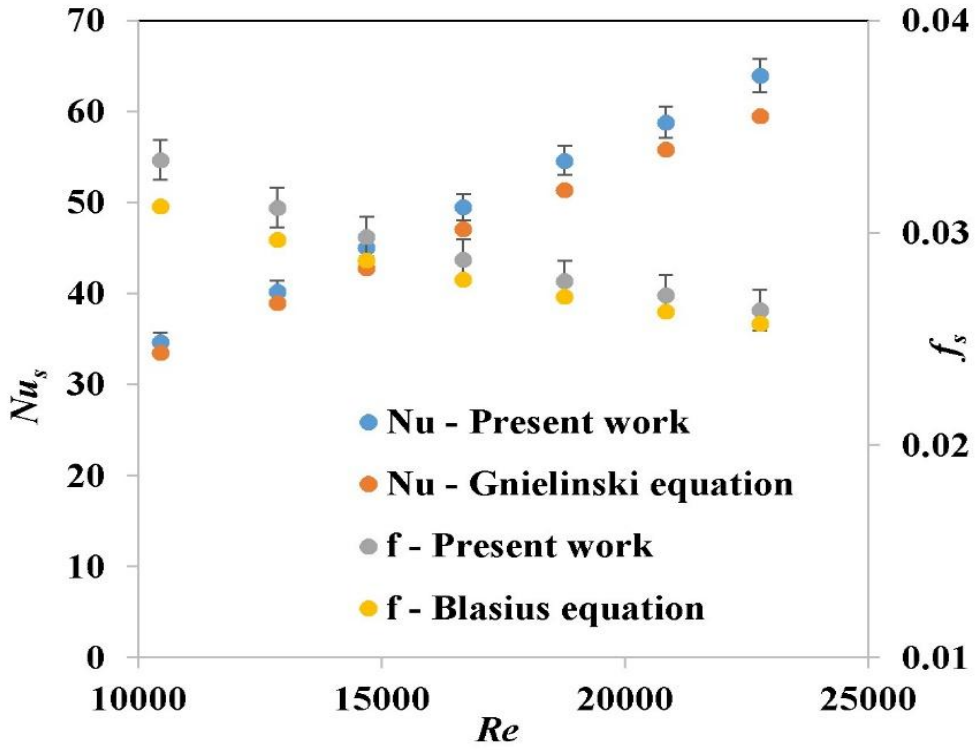


Figure 3: Plots for experimental system validation.

5. Thermo-hydraulic performance

To analyse the data in the form of dimensionless number, viz., Nusselt number and friction factor, the plots of Nusselt number (Nu), friction factor (f), Nusselt number enhancement ratio (Nu/Nu_s), and thermal performance factor (η) are plotted for various tapes.

5.1 Variation of the Nusselt number (Nu)

Figure 4 shows the Nu plot for various twisted tape geometries. The Nu increases with Re in all cases, however Nu climbs up in the order of STT, PTT, DSTT, DPTT, DPTT with V-winglet irrespective of the Re. A considerable rise in Nu is observed for DPTT with V-winglet compared to other tape geometries. Double twisted tape having counter-swirl orientation depicts higher Nu. An increase in the twist ratio of twisted tape adversely affects the Nusselt number in all cases. A comparative evaluation of the Nusselt number plots at 3 different twist ratios reveals a greater impact of Reynolds number on the Nusselt number as the twist ratio of tape increases.

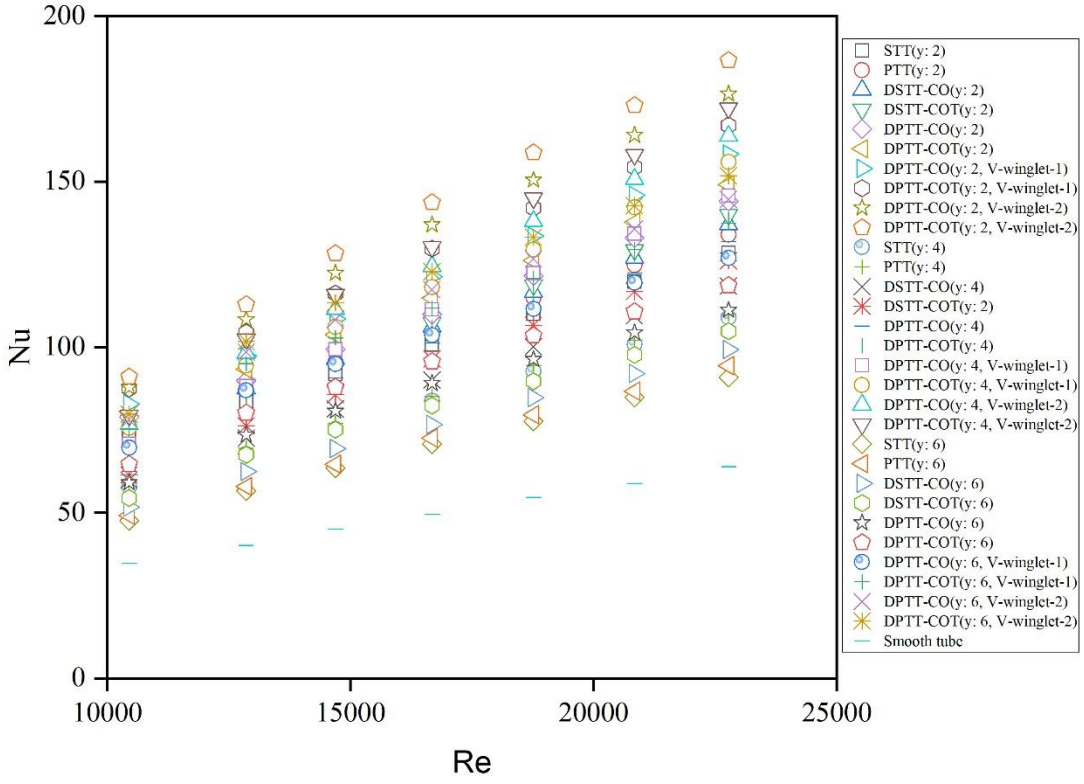


Figure 4: Performance characteristics for various twisted tape configurations.

5.2 Friction factor variation characteristics

The effect of insert geometry on friction factor (*f*) is assessed in Figure 5. The friction factor remains highest for the DPTT with V-winglet geometry. A higher sensitivity in friction factor is seen at low *Re* where it is clearly reflected that the perforations bring down the friction while a counter-swirl orientation of double tape causing greater friction. The effect of varying twist ratio can be perceived from the plots: Increasing twist ratio from 2 to 4 leads to a significant reduction in the friction factor in all cases, however, further increase in the twist ratio from 4 to 6 shows a further reduction in friction factor but not up to the level of previous case.

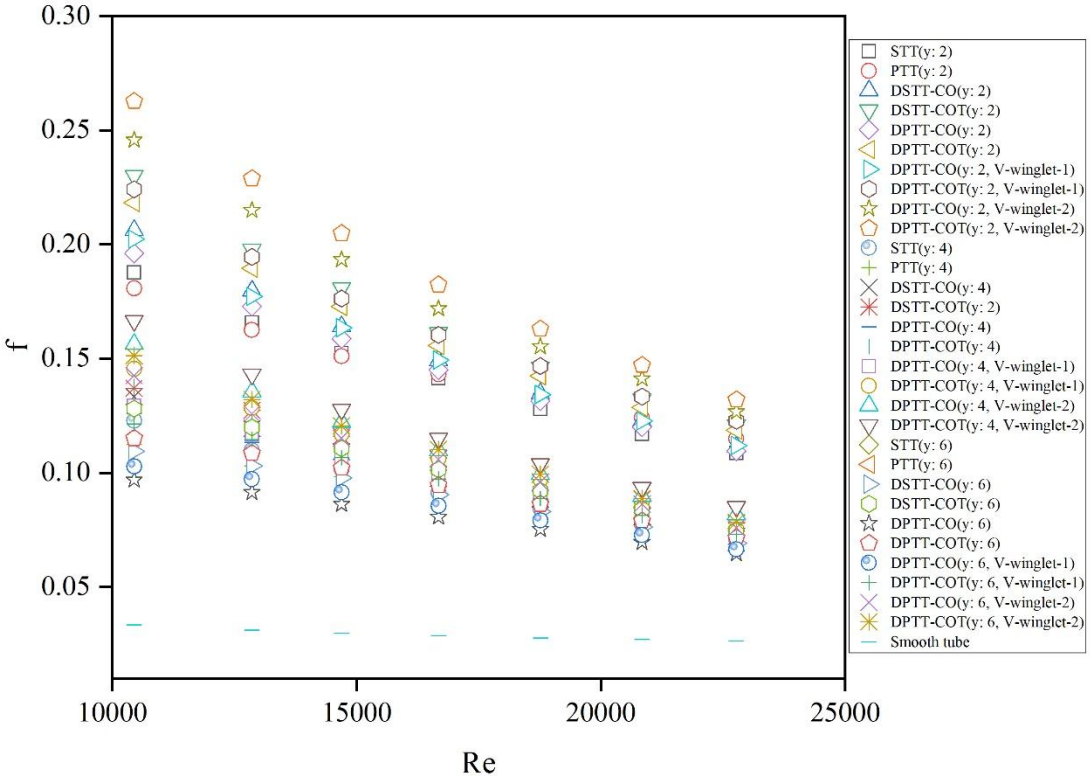


Figure 5: Friction factor (f) characteristics for various twisted tape configurations.

5.3 Thermo-hydraulic performance factor (η)

Most of the heat transfer enhancement techniques invite frictional losses due to fluid turbulence. The net outcome is quantified by thermal performance factor (η) as given in equation 6. The desired value of η is more than unity, which is attained by all geometries of twisted tape. The DPTT-COT with V-winglet surpasses other tapes by a considerable margin as shown in Figure 6. The maximum value of (η) is found to be 1.82 for DPTT-COT with V-winglet. Moreover, this geometry of twisted tape brings a 16.4% rise in η as *Re* varies from 10400 to 22800, which is highest among all cases.

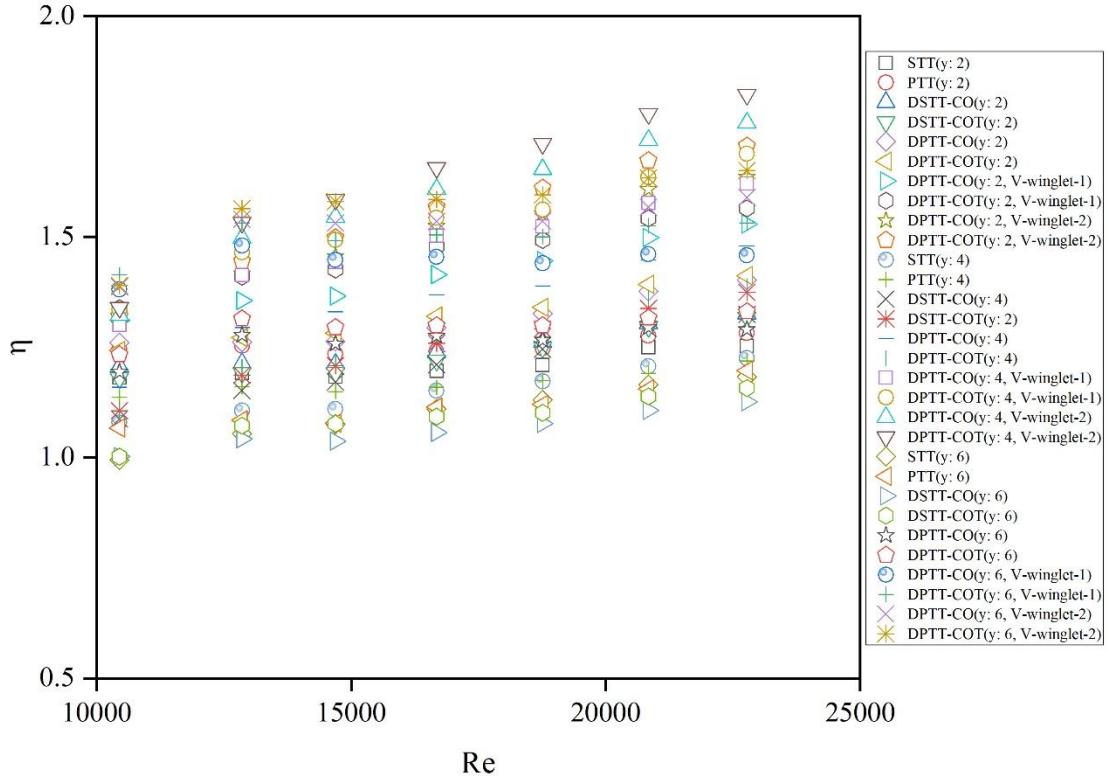


Figure 6: Thermal performance factor (η) for various twisted tape configurations.

5.4 Dimensionless entropy generation parameter (N_s)

The variation of entropy generation number for all insert geometries is shown in Figure 7. The entropy generation either increases or remains unaffected with the change in Reynolds number. The double perforated twisted tape with counter orientation (V-winglet-1) and y = 6 demonstrates the minimum entropy generation, exhibiting the most suitable insert geometry among all investigated cases.

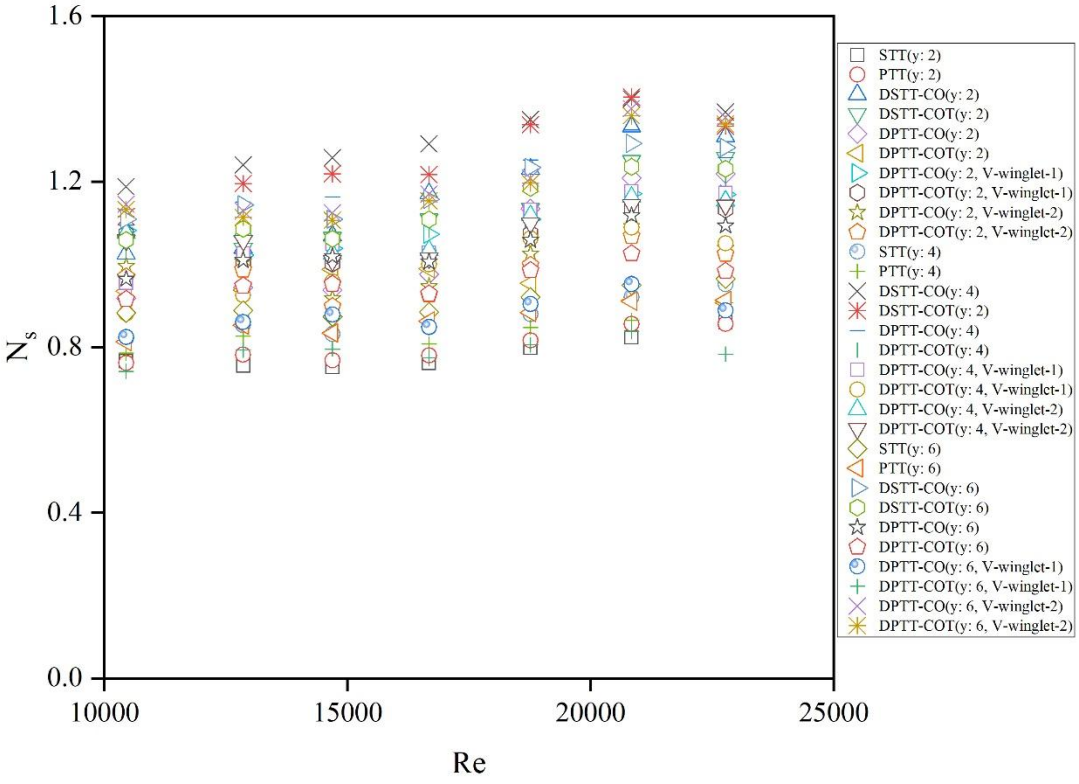


Figure 7: Entropy generation number (Ns) for various twisted tape configurations.

6. Machine learning framework for thermo-hydraulic prediction and multi-objective optimization

This section presents a multi-model machine learning, explainable artificial intelligence (XAI) and multiobjective optimization-based comprehensive data-driven framework to predict and optimize the thermo-hydraulic performance of twisted tape configurations. The generated dataset includes the most important operational and geometrical parameters, such as Reynolds number (Re), tape pitch ratio (y), and tape configurations, and the results are Nusselt number (Nu), friction factor (f), thermal performance factor (eta), and entropy generation number (N_s). The five machine learning models (MLR, RF, XGBoost, LS-SVM and ANN) were trained and assessed with LS-SVM and XGBoost performing better with higher predictive accuracy with high R^2 (0.99) and lower prediction error on all outputs. Parity analysis, REC curves and cross-validation methods are employed to test the proposed models. Interpretability and physical consistency of the machine learned relationships are further verified by SHapley Additive exPlanations (SHAP). A multi-objective optimization analysis using NSGA-II algorithm is performed to optimal conditions of achieving higher heat transfer with the low to moderate frictional losses.

6.1 Proposed methodology

To examine the thermo-hydraulic behaviour of twisted tapes, a data-driven integrated framework is developed. The experimental data is processed through the controlled machine learning modeling, explainable artificial intelligence (XAI), and multi-objective optimization. This integrated approach can accurately determine the key performance parameters such as, Nusselt number, friction factor, thermal performance factor as well as the entropy generation number Moreover, it also help critically evaluate the optimal set of system and operating parameters. The proposed machine learning methodology has four components: (i) data preparation and preprocessing, (ii) model generation and testing, (iii) interpretability and feature attribution of a model using SHAP, and (iv) multi-objective optimization using genetic algorithm.

6.1.1 Experimental Dataset Description

The data that will be used in this research is based on controlled experimental research studies carried out on a circular tube heat exchanger with different twisted tape inserts. The main aim of the experiments was to test the thermohydraulic performance of various geometry and flow conditions. The data set collected is used to model and optimize supervised machine learning. The operating and geometric variables make the input parameters. The Reynolds number (*Re*) is the operating condition that defines the flow regime in the tube. The geometry of the insert is determined by two parameters: the twist ratio (*y*) and the type of the tape (categorical variable representing the particular twisted tape geometry, modified and winglet geometry). These parameters regulate the intensity of mixing of the flow and disturbance of the boundary layers within the tube. The experimental results of the output parameters are:

- Nusselt number (*Nu*): the measure of the increase in heat transfer due to convection,
- Friction factor (*f*): indicating the pressure drop penalty due to insert-induced turbulence,
- Thermal performance factor (η): the overall improvement of heat transfer, compared to the pressure drop,
- Entropy generation number (N_s): measurement of thermodynamic irreversibility in the system.

Each data point is thus a structured mapping:

$$(\mathrm{Re}, \mathrm{y}, \mathrm{TapeType}) \rightarrow (\mathrm{Nu}, \mathrm{f}, \eta,\ \mathrm{N}_s) \tag{1}$$

Numerical values were examined to be within experimentally relevant, realistic ranges that the heat transfer factors behaviour was monotonic with increasing Reynolds number and friction factor patterns are realistic. The categories insert types were coded to be used in computational modelling and still have physical interpretation. The data recreates the multi-process hydraulic and thermal behaviour, permitting predictive modelling and, multi-objective optimization. Its design facilitates regression-based learning and allows interpretability in line with thermo-fluid concepts.

6.1.2 Data Preprocessing

To find the numerical stability, model generalization, and physical consistency of the experimental data, the preprocessing of the experimental data was performed systematically. The preprocessing process involved four major steps such as data cleaning, categorical variable encoding, feature scaling, and partitioning data.

1) Data Cleaning and Consistency Check: Any numerical variable was reviewed with regard to missing values and odd values. Whereby, n is the number of samples, p is the number of features considered as inputs and q is the number of features considered as outputs. Incomplete numerical data, where available, was filled with the median value of the feature to maintain the distributional properties without bias. Monotonic trends between *Re* and *Nu* were used to check physical consistency, and the realistic magnitude of f and N_s were checked to be within experimentally significant limits.

2) Categorical Encoding: The twisted tape (TapeType) is a categorical variable. One-hot encoding was used to include this variable in machine learning models using regression. Assuming there exist k different insert geometries, then the categorical variable is converted into a binary vector, **z** in the form of a binary vector, i.e. 0, 1, i.e.:

$$z_i \begin{cases} 1, \text{ if the sample belongs to category } i, \\ 0, \text{ otherwise.} \end{cases} \tag{2}$$

This transformation maintains the geometrical identity and makes it possible to compute numerically.

3) Feature Scaling: Numerical inputs were z-score normalized to remove the difference in scale among variables:

$$x_{scaled} = \frac{x - \mu_x}{\sigma_x} \tag{3}$$

and where, the mean and standard deviation of feature x are represented by μ_x and σ_x, respectively. This normalization augments convergence behaviour of gradient based models like artificial neural networks and support vector regression.

4) Dataset Partitioning: An 80:20 split ratio was used to divide the dataset into two subsets (training and testing). Furthermore, cross validation of five times was used to train the model to assess the generalization ability. In k-fold cross validation, the data are divided into k discontinuous subsets and the model is trained k times, with one of these subsets being used to validate the model, and the other subsets used as the training set. This preprocessing structure guarantees numerical resiliency, minimizes the chances of overfitting, and preserves interpretability in accordance with thermo-hydraulic concepts.

6.1.3 Machine Learning Model Development

To model the nonlinear relationship between thermohydraulic operating conditions and performance indicators, multiple supervised regression algorithms were implemented. Each model was trained to learn the functional mapping:

$$f_\theta : \mathrm{R}^p \rightarrow \mathrm{R}^q \tag{4}$$

where R^p represents the input feature space (Re, twist ratio, encoded tape type), and R^q denotes the predicted outputs (Nu, f, η, and N_s). The parameter vector θ corresponds to model specific trainable parameters.

1) Multiple Linear Regression (MLR): Multiple Linear Regression assumes a linear relationship between inputs and outputs. For a given response variable y, the model is expressed as:

$$y = \beta_0 + \sum_{i=1}^{p} \beta_i x_i + \epsilon \tag{5}$$

where β_0 is the intercept, β_i are regression coefficients, x_i are input variables, and ϵ represents the residual error term.

The model parameters are estimated by minimizing the ordinary least squares (OLS) objective:

$$\min\beta \sum_{j=1}^{n} \left(y_j - \hat{y}_j\right)^2 \tag{6}$$

MLR serves as a baseline model for evaluating the benefits of nonlinear learning approaches.

2) Random Forest (RF): Random Forest is an ensemble learning method based on bootstrap aggregation and decision trees. The model constructs multiple regression trees using random subsets of data and features. The final prediction is obtained by averaging individual tree outputs:

$$\hat{y} = \frac{1}{T}\sum_{t=1}^{T} h_t(x) \tag{7}$$

where T is the number of trees and $h_t(x)$ denotes the prediction from the t-th tree. Random feature selection and bootstrapping reduce variance and improve generalization, making RF effective for capturing nonlinear thermo-hydraulic interactions.

3) Artificial Neural Network (ANN): A feedforward Artificial Neural Network with backpropagation was implemented to model complex nonlinear relationships. For a network with L layers, the transformation at layer l is defined as:

$$\mathrm{a}^{(l)} = \sigma\left[\mathrm{W}^{(l)}\mathrm{a}^{(l-1)} + \mathrm{b}^{(l)}\right] \tag{8}$$

where: $\mathrm{W}^{(l)}$ and $\mathrm{b}^{(l)}$ are weights and biases, $\sigma(\cdot)$ denotes the activation function (ReLU), $\mathrm{a}^{(l)}$ is the output of layer l.

The network parameters are optimized by minimizing the mean squared error (MSE):

$$\mathcal{L} = \frac{1}{n}\sum_{j=1}^{n}\left(y_j - \hat{y}_j\right)^2 \tag{9}$$

using gradient-based backpropagation. ANN enables flexible approximation of nonlinear thermo-fluid dynamics without explicit physical modeling.

4) Extreme Gradient Boosting (XGBoost): XGBoost is a gradient boosting ensemble method that builds additive regression trees sequentially. The prediction at iteration k is expressed as:

$$\hat{y}^{(k)} = \sum_{t=1}^{k} f_t(x) \tag{10}$$

where each $f_t(x)$ represents a regression tree trained to minimize the regularized objective:

$$\mathcal{L} = \sum_{i=1}^{n} l(y_i, \hat{y}_i) + \sum_{t=1}^{k} \Omega(f_t) \tag{11}$$

Here, $l(\cdot)$ denotes the loss function (squared error), and $\Omega(f_t)$ is a regularization term controlling tree complexity:

$$\Omega(f) = \gamma \mathrm{T} + \frac{1}{2}\lambda\sum_{j=1}^{T}{\omega_j}^2 \tag{12}$$

where T is the number of leaves and ω_j are leaf weights. Regularization prevents overfitting and enhances predictive stability. Due to its ability to capture high-order feature interactions, XGBoost is particularly suitable for thermo-hydraulic performance modelling.

5) Model Validation Strategy: All models were evaluated using an 80:20 train-test split along with five-fold cross- validation. Performance metrics included R^2, mean absolute error (MAE), and root mean square error (RMSE). This multi-model framework enables rigorous comparison between linear, ensemble, and neural approaches for predicting heat transfer and flow performance indicators.

6.1.4 Explainable Artificial Intelligence: SHAP Analysis

While ensemble and neural network models provide high predictive accuracy, their internal decision-making process is often non-transparent. To enhance interpretability and ensure physical consistency of the learned relationships, SHapley Additive exPlanations (SHAP) were employed to quantify feature contributions to model predictions.

1) Shapley Value Formulation: SHAP is grounded in co-operative game theory, where each input feature is treated as a "player" contributing to the final prediction. For a given prediction $f(x)$, the Shapley value ϕ_i for feature i is defined as:

$$\phi_i = \sum (S \subseteq F \setminus i)(|S|!\,(|F| - |S| - 1)!)/(|F|!)\left[f_{(S\cup i)}\left(x_{(S\cup i)}\right) - f_S(x_S)\right] \quad (13)$$

where: F denotes the set of all input features, S represents a subset of features excluding feature i, $f_S(x_S)$ is the model prediction using only the feature subset S, |S| is the cardinality of subset S. The Shapley value ϕ_i represents the average marginal contribution of feature i across all possible coalitions of features.

2) Additive Explanation Model: SHAP approximates the model locally using an additive explanation model:

$$f(x) = \phi_0 + \sum (i = 1)^p \phi_i \quad (14)$$

where: ϕ_0 is the expected model output over the dataset, ϕi represents the contribution of feature i to the deviation from the expected prediction. This formulation ensures consistency and local accuracy, meaning the sum of feature contributions equals the model output for each instance.

3) TreeSHAP Implementation: For tree-based models such as Random Forest and XGBoost, the TreeSHAP algorithm was employed. TreeSHAP computes exact Shapley values in polynomial time by

exploiting the hierarchical structure of decision trees, significantly reducing computational complexity compared to brute-force enumeration.

4) Global Feature Importance: Global feature importance was assessed by computing the mean absolute Shapley value:

$$I_i = 1/n \sum (j = 1)^n \left| \phi_i^{(j)} \right| \quad (15)$$

where $\phi_i^{(j)}$ denotes the Shapley value of feature i for sample j. Larger I_i values indicate stronger influence on the model output.

5) Feature Interaction Effects: To analyze coupled thermo-hydraulic behavior, SHAP dependence plots were generated to visualize interaction effects, particularly between Reynolds number (Re) and twisted tape configuration. Interaction analysis enables identification of nonlinear amplification effects where geometric modifications influence heat transfer differently across flow regimes.

6) Physical Consistency Verification: The SHAP analysis was further examined to ensure alignment with thermo- fluid theory. For instance, positive Shapley contributions of Reynolds number to Nusselt number confirm enhanced convective heat transfer at higher flow rates. Similarly, friction factor contributions were evaluated to verify realistic pressure drop behavior. By integrating SHAP-based interpretability with high-performance predictive modeling, the proposed framework ensures both accuracy and transparency, strengthening the re- liability of machine learning-driven thermo-hydraulic analysis.

6.1.5 Multi-Objective Optimization using NSGA-II

The thermo-hydraulic performance of twisted tape-enhanced heat exchanger tubes inherently involves competing objectives. While increasing Reynolds number and geometric modification may enhance heat transfer (higher Nu), they simultaneously increase pressure drop (higher f) and entropy generation (N_s). Therefore, a multi-objective optimization framework was implemented to identify optimal trade-off solutions. The optimization problem is formulated as:

$$\begin{aligned} &Maximize f_1(x) = Nu(x) \\ &Maximize f_2(x) = \eta(x) \\ &Minimize f_3(x) = f(x) \\ &Minimize f_4(x) = N_s(x) \end{aligned} \quad (16)$$

subject to:

$$x = Re, y, \text{TapeType} \quad (17)$$

$$Re_{min} \leq Re \leq Re_{max} \tag{18}$$

$$y_{min} \leq y \leq y_{max} \tag{19}$$

where the bounds are derived from experimentally observed operating conditions. Since the objectives are conflicting, no single global optimum exists. Instead, a set of Pareto-optimal solutions is obtained.

1) Pareto Optimality: The solution x^* is a Pareto optimal when there is no other solution of the form x where:

$$f_i(x) \leq f_i(x^*) \forall i \tag{20}$$

with strictly one inequality. The set of all these nondominated solutions is the Pareto front, which indicates the best trade-offs between heat transfer enhancement and flow penalty.

2) NSGA-II Algorithm: Non-dominated Sorting Genetic Algorithm II (NSGA-II) was adopted since it is computationally efficient and can preserve diversity of solutions. The algorithm will work in the following steps: Initialization: Generate an initial population of candidate solutions within the feasible parameter space. Fitness Evaluation: Evaluate each candidate using trained machine learning models to predict Nu, f, η, and Ns. Non-dominated Sorting: Rank solutions based on Pareto dominance levels. Crowding Distance Assignment: Compute crowding distance to preserve diversity across the Pareto front. Selection, Crossover, and Mutation: Generate offspring using genetic operators. Elitism: Combine parent and offspring populations and select the best individuals for the next generation.

The dominance ranking ensures convergence toward optimal trade-off solutions, while crowding distance prevents premature clustering of solutions.

The problem to be integrated with Machine Learning Models is described as follows.

The trained machine learning models were substituted in the optimization loop as surrogate predictors instead of the direct evaluation of the computational fluid dynamics simulations:

$$f_i(x) = \mathrm{M}_i(x) \tag{21}$$

In which, the predictive model trained on each objective is denoted as, M_i. This surrogate-based optimization saves a lot on computational cost and does not affect predictive accuracy.

6.1.6 *Optimization Output:* This algorithm provides a Pareto front about the optimum combinations of Reynolds number, twist ratio, and insert type. These solutions allow engineers with design options that are flexible with either emphasis on maximum heat transfer, minimum pressure drop or balanced thermo-

hydraulic efficiency. The proposed framework, the combination of machine learning prediction and evolutionary multi-objective optimization, allows the design of a thermal system based on real-world engineering constraints.

6.2 Experimental Dataset Description

The data used in this research is based on the controlled experimental research carried out on a circular tube heat exchanger with different twisted tape inserts. The aim of the experimental campaign was to measure the thermo-hydraulic performance of various flow and geometric conditions.

The primary input parameters that should be taken into account in the current analysis are the Reynolds number (Re), the twist ratio (y), and the type of insert (when considered as categorical types of tapes). Reynolds number is used to explain the flow regime and regulate the convective heat transfer behaviour and the twist ratio regulates the geometric change caused by twisted tape. Different structural configurations are denoted in the type of insert, hence influencing the swirl intensity and disturbance of the boundary layer. The performance indicators of the output that are measured experimentally are:

- Nusselt number (Nu), representing the convective heat transfer enhancement,
- Friction factor (f), quantifying the pressure drop penalty,
- Thermal performance factor (η), indicating the overall enhancement efficiency,
- Entropy generation number (N_s), evaluating thermodynamic irreversibility.

All experimental observations were done in steady-state operating conditions. The data range covers a large range of Reynolds numbers to cover sufficient laminar-turbulent transition regimes that are applicable in real-life heat exchanger environments. Before the implementation of machine learning, the dataset was checked for consistency, outliers, and absence of entries to verify the physical reliability and statistical validity.

The hydrodynamic, thermal, and thermodynamic performance parameters are combined to help comprehensively evaluate heat transfer augmentation strategies. The following machine learning modeling and multi-objective optimization framework in this work is based on this dataset.

6.3 Performance Evaluation of Machine Learning Models

The predictive performance of the developed models was measured by various statistical measures, such as the coefficient of determination (R^2), mean squared error (MSE), root mean square error (RMSE), mean absolute error (MAE), and mean absolute percentage error (MAPE). The statistics are used to give supplementary information on the accuracy and stability of the models to various output variables, i.e. Nu, f,

η, and N_s. Coefficient of determination (R^2) is a measure of how much the target variable is explained by the model and it is expressed as:

$$R^2 = 1 - \left(\sum (i=1)^n (y_i - \hat{y}_i)^2\right) / \left(\sum (i=1)^n (y_i - \bar{y})^2\right) \quad (22)$$

In which, y_i is the actual value, $\hat{y}_i$ is the predicted value, $\bar{y}$ is the mean of the observed values and n is the number of samples. RMS error gives an indication of the average strength of the error in prediction and it can be defined as:

$$RMSE = \sqrt{\left(1/n \sum (i=1)^n (y_i - \hat{y}_i)^2\right)} \quad (23)$$

Equally, the MAE is the mean of the absolute differences between the actual and predicted values:

$$MAE = 1/n \sum (i=1)^n |y_i - \hat{y}_i| \quad (24)$$

To capture the relative error in percentage terms, MAPE is used:

$$MAPE = 100/n \sum (i=1)^n |(y_i - \hat{y}_i)/y_i| \quad (25)$$

The value of R^2 and the values of RMSE, MAE and MAPE are lower, which is a sign of a good predictive performance.

6.4 Comparative Performance Across Models

The findings illustrated in Table I results are clearly shown to show that there is no given model that outshines all other outputs but some tendencies are apparent. To predict *Nu*, the BPNN model performed best in terms of R-Squared (0.9917) and lowest RMSE, which implies that it has a high learning ability in predicting the behaviour of heat transfer. Nevertheless, the lowest MAPE was given by LS-SVM, which indicates a slightly better relative accuracy. Moreover, ELM was found to perform better in terms of R^2, RMSE and LS-SVM was found to perform best in terms of MAE and MAPE in case of friction factor as well (f). This implies that the two models are very effective with LS-SVM being more stable in error distribution. In addition, XGBoost had the lowest percentage error, whereas BPNN had the highest R^2 with respect to thermal efficiency (η). This low efficiency of ELM to predict the underlying relationship is a limitation to the efficiency prediction because its performance on this output is rather poor. Entropy generation prediction (*Ns*) seems to be the most difficult. Despite this, LS-SVM was always the best performing models in all the metrics with the highest accuracy and minimum error values. This is a strength of this model in complex thermodynamic behaviour modelling. Figure 1 displays a comparison of all the models worldwide in terms of normalized R^2 and inverted RMSE averaged over all the outputs (*Nu*, *f*, η, and N_s). The bigger enclosed areas of XGBoost and LS-SVM

suggest that they have the best overall predictive accuracy, whereas MLR and RF have much lower accuracy and larger error.

In general, the comparative analysis shows that ensemble based models like Random Forest and XGBoost tend to perform better in predicting the data because of their capacity to learn nonlinear relationships and convoluted interactions between input features. The models based on neural networks also show competitive behaviour especially in cases of highly nonlinear outputs. Conversely, linear models like MLR exhibit relatively lower accuracy, as a demonstration of the constraints of the linear assumptions in the current problem.

TABLE I: Comparative performance of machine learning models for all output responses

Output	Model	R^2	MSE	RMSE	MAE	MAPE (%)
Nu	RF	0.9415	58.0248	7.6174	5.9522	5.8757
	XGBoost	0.9895	10.4513	3.2328	2.4503	2.2146
	LS-SVM (KRR-RBF)	0.9899	10.0623	3.1721	1.9105	**1.6361**
	ELM	0.9867	13.2261	3.6368	2.1448	2.4706
	BPNN	**0.9917**	**8.2436**	**2.8712**	2.0257	1.9903
f	RF	0.8830	0.0001	0.0107	0.0085	7.9265
	XGBoost	0.9738	0.0000	0.0051	0.0035	3.1720
	LS-SVM (KRR-RBF)	0.9760	0.0000	0.0049	**0.0021**	**1.7298**
	ELM	**0.9929**	0.0000	**0.0026**	0.0020	1.9597
	BPNN	0.9779	0.0000	0.0047	0.0027	2.4577
η	RF	0.9648	0.0013	0.0364	0.0290	2.1336
	XGBoost	0.9875	0.0005	0.0217	0.0174	**1.2923**
	LS-SVM (KRR-RBF)	0.9765	0.0009	0.0298	0.0204	1.4615
	ELM	0.7964	0.0077	0.0877	0.0531	4.1151
	BPNN	**0.9812**	0.0007	0.0267	0.0191	1.4280
N_s	RF	0.8001	0.0039	0.0624	().0499	4.6941
	XGBoost	0.9353	0.0013	0.0355	0.0299	2.7899
	LS-SVM (KRR-RBF)	**0.9441**	**0.0011**	**0.0330**	**0.0249**	**2.3051**
	ELM	0.8113	0.0037	0.0606	0.0484	4.5743
	BPNN	0.9239	0.0015	0.0385	0.0308	2.8760

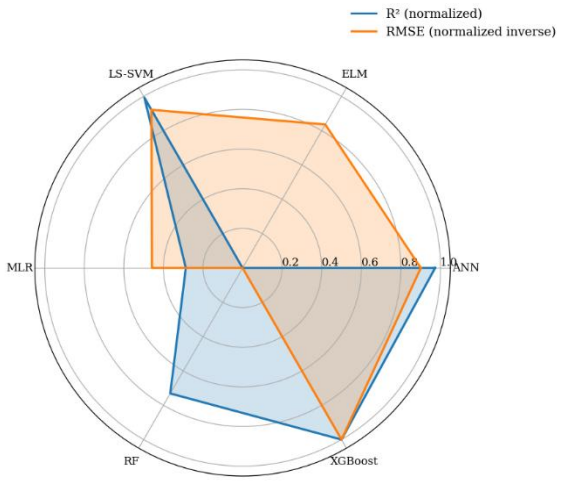


Figure 8: Performance comparison of machine learning models using normalized R^2 and inverted RMSE.

6.5 Correlation Analysis of Model Predictions

Along with the quantitative measures of error, a visual and statistical analysis was also conducted to gain a better insight into the associations between variables and predictive behaviour of the chosen model. This includes (i) correlation analysis of input-output variables and (ii) parity analysis between experimental and predicted values.

Figure 9 shows the correlation heatmap between the governing parameters and output responses in the form of a Pearson correlation. The correlation coefficients are between −1 and +1 which shows the strength and direction of linear relationships. As can be seen, Reynolds number (Re) is positively correlated with the Nusselt number (Nu) (0.7483), which implies that the dynamics of the flow has a considerable impact on the enhancement of the heat transfer. Conversely, the friction factor (f) is strongly negatively correlated with both Re (−0.5428) and the channel parameter, y (−0.7043), meaning the lower the flow intensity and geometric variation the lower is the resistance to the flow. Thermal performance factor (η) has a positive correlation with Nu (0.6262) as is natural since better heat transfer will have a direct impact on the performance. Entropy generation number (N_s) demonstrates moderate correlations with Re, Nu, f and weak correlations with the other variables which indicates the rather intricate and non-linear character of the phenomena associated with entropy. In general, the correlation analysis proves that the chosen input parameters are appropriate and have significant connections with the output responses, which justifies their application in the model development.

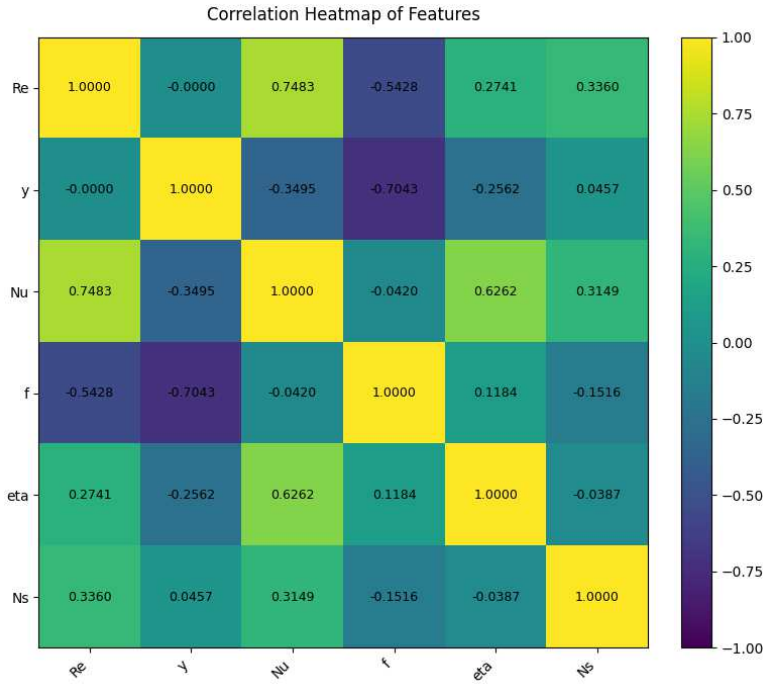


Figure 9: Pearson correlation heatmap showing relationships among input parameters and output responses.

6.6 Effect of Tape Type on Output Responses

Fig. 10 shows how various twisted tape geometries affect the thermo-hydraulic performance. Clearly, designs with V-winglet designs, especially DPTT-COT (V-winglet-2) designs, have greatly improved heat transfer performance with the highest Nusselt number (Nu = 130.644) and better thermal performance factor (η = 1.583). Nonetheless, this improvement is accompanied by a commensurate rise in friction factor meaning that there is a trade-off between heat transfer augmentation and flow resistance. Conversely, less complex designs like STT and PTT have lower heat transfer capacity, but also less frictional losses. It is noteworthy that some of the configurations such as DPTT-COT (V-winglet-1) show a comparatively balanced performance with moderate Nu and lower entropy generation (N_s), indicating better thermodynamic efficiency. Altogether, the findings indicate that the geometric changes, especially the incorporation of winglet patterns, are important in promoting the convective heat transfer and affecting the hydraulic and entropy properties, thus, establishing the importance of optimum design trade-offs in thermal system applications.

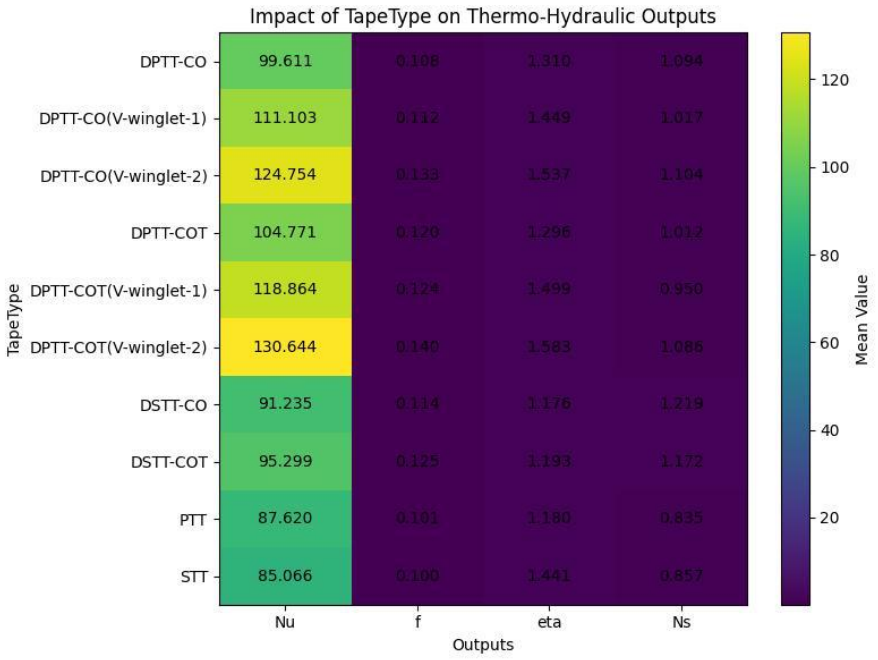


Figure 10: Effect of different twisted tape configurations on thermo-hydraulic performance parameters.

6.7 Parity Analysis: Experimental vs Predicted Values

In order to further evaluate the predictive power of the models created, a parity analysis was conducted by comparing experimental values with resultant predictions made by various machine learning models, such as MLR, RF, XGBoost, LSSVM, ELM, and ANN. Parity plots offer a visual analogy of the proximity of the predictions to the ideal condition, as opposed to statistical measures. The solid diagonal line in both plots shows the optimal agreement (y = x) and the dotted lines show the upper and lower limits of the deviation by 10 percent. These predictions are deemed to be acceptable in engineering applications. To further compare predictive performance, the parity analysis was further expanded not just to a single-model analysis Figure 11 but also to a multi-model framework Figure 12 allowing direct visual comparison of all the models with the experimental observations.

The predicted values of *Nu* are highly consistent with the experimental values in all models. All data points lie close to the ideal line, which means that the heat transfer characteristics are predicted properly. LS-SVM, BPNN and XGBoost have closer clusters with less scattered values, but MLR and RF exhibit a slight greater deviation, especially at large values of *Nu*.

1) The predicted values of *f* are tightly clustered around the ideal line meaning that it performs in a consistent and reliable manner. The dispersion of the data points is low relative to other outputs implying that

the model of f is comparatively simpler. The higher-order models, including LS-SVM and XGBoost are better aligned with the range of 10% on each side, whereas standard models are more dispersed. A higher diffusivity of predicted values of η than that of Nu and f suggesting moderate complexity in the representation of thermal performance behaviour. LS-SVM and ANN exhibit a relatively higher agreement whereas ELM exhibits some deviations. The comparison of the prediction of Ns has a relatively higher scatter among all the models since the generation of entropy is a complicated and non-linear process. Even though the majority of data points continue to adhere to the overall pattern of the ideal line, some of the predictions are outside the range of 10%. LS-SVM is more consistent, whereas other models are more variable in some circumstances.

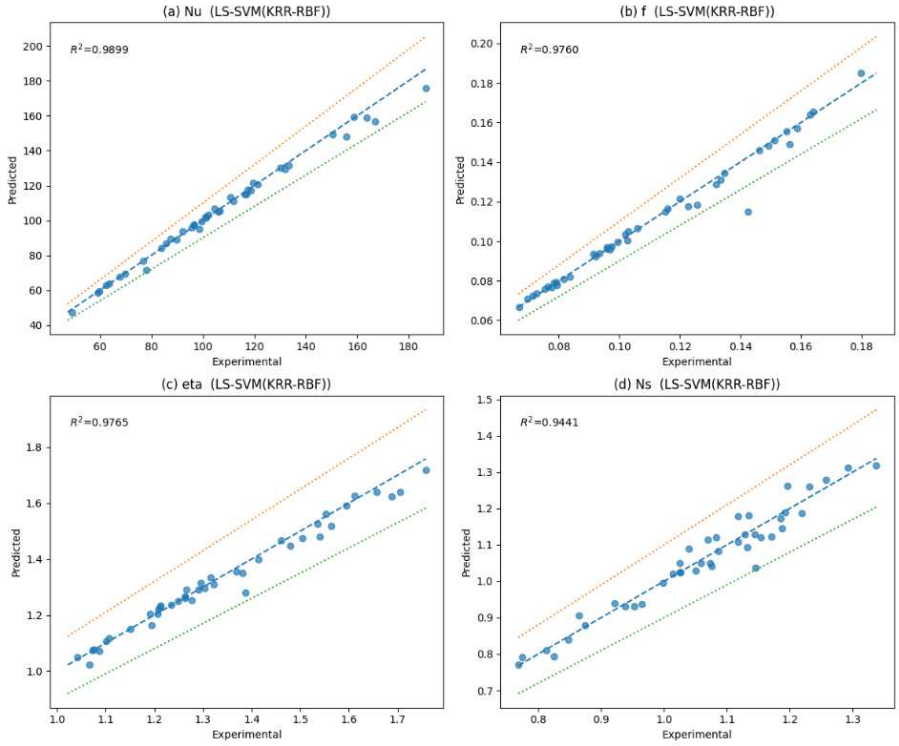


Figure 11: Parity plots for (a) Nu, (b) f, (c) η, and (d) N_s.

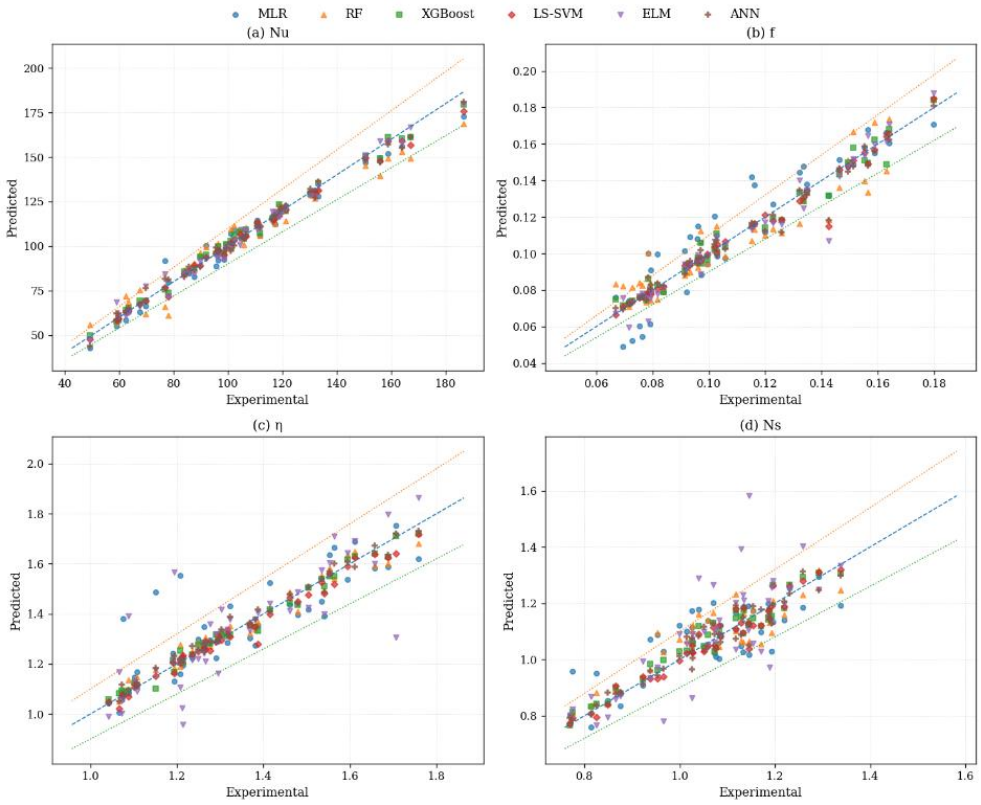


Figure 12: Multi-model parity plots for (a) Nu, (b) f, (c) η, and (d) N_s.

6.8 Error Analysis and Model Reliability

Although general accuracy measures give an overview of how well a model can predict, to have a more insight into the quality of predictions, it is necessary to examine the distribution and behaviour of errors. The error analysis in this research was conducted with the help of histogram-based distribution analysis, boxplot-based visualization and residual analysis on all output variables. This aids in detecting biasness, variability and extreme deviations.

The distribution of actual and predicted values for each output variable is illustrated in Figure 13. The histograms overlap with each other indicating that the experimental and predicted distributions greatly agree especially at the values of *Nu* and f where the shapes of the two distributions closely match. In the case of thermal performance factor (η) and entropy generation number (N_s), the distributions of the predictions follow the overall trend of the real data, but some minor spreading is noticed. This shows that the overall behaviour is well captured by the model with a few deviations at some ranges. More information is gained on the relative error histograms (Figure 14), where the error values are clumped around zero. This implies that the model is not systematic and predicts in a balanced manner. The fact that the range of errors of *Nu* and *f* are narrow, as

opposed to that of N_s, shows that the errors in prediction are more stable, but N_s has a more widespread range, demonstrating its complexity.

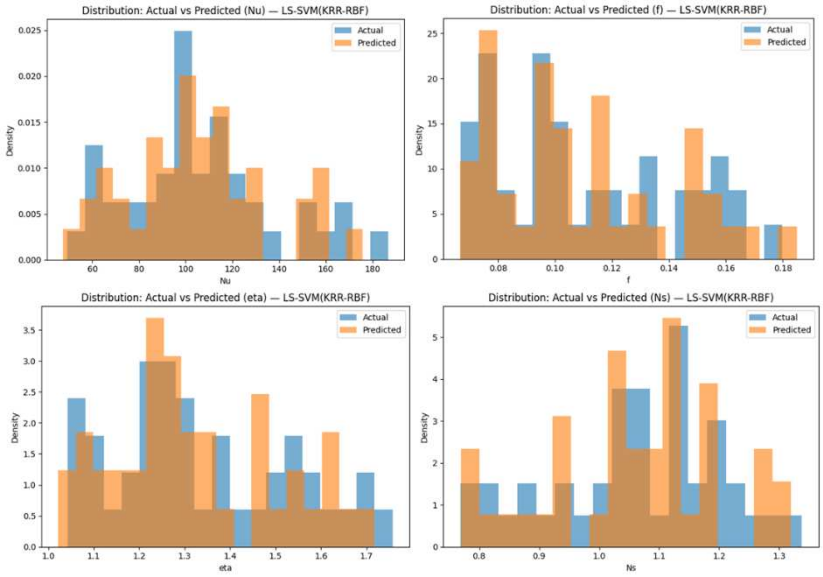


Figure 13: Comparison of probability density distributions between experimental (actual) and predicted values for (a) Nu, (b) f, (c) η, and (d) N_s using the LS-SVM (KRR-RBF) model.

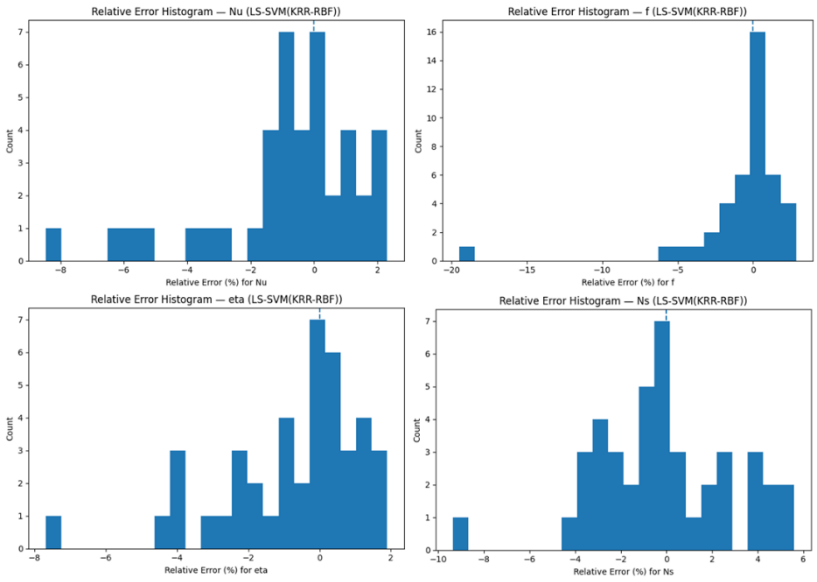


Figure 14: Relative error distribution (%) of LS-SVM (KRR-RBF) model predictions for (a) Nu, (b) f, (c) η, and (d) N_s.

Figure 15 illustrates a box plot analysis of the errors in prediction to study the dispersion and central tendency of the error values of each output variable as depicted in Fig. 8. It can be noted that LS-SVM and BPNN tend to have narrower interquartile ranges and medians near zero, which means a smaller bias and a higher

consistency. Conversely, the variability of Random Forest is bigger, especially in the case of *Nu* when the range of errors is much broader. All models have relatively compact error distributions for friction factor (*f*), which substantiates the fact that the parameter is easier to predict. But in the case of entropy generation (N_s) the distribution is broader over all models and outliers occur, which emphasizes the greater complexity of modelling entropy-related behaviour.

The Residual analysis was also performed to determine the randomness of prediction errors or whether there are systematic patterns. Ideally, the residuals would be symmetrically distributed about zero with no noticeable trend. The findings show that the residual of *Nu*, *f*, and η is mainly centred on the value of zero meaning that the models are not characterised by consistent underestimation or overestimation. It confirms that the underlying patterns of data have been captured through the learning process. But the residuals are dispersed with N_s which is consistent with previous findings with parity and error distribution plots. This is not surprising since many interacting parameters affect the generation of entropy and it is more nonlinear.

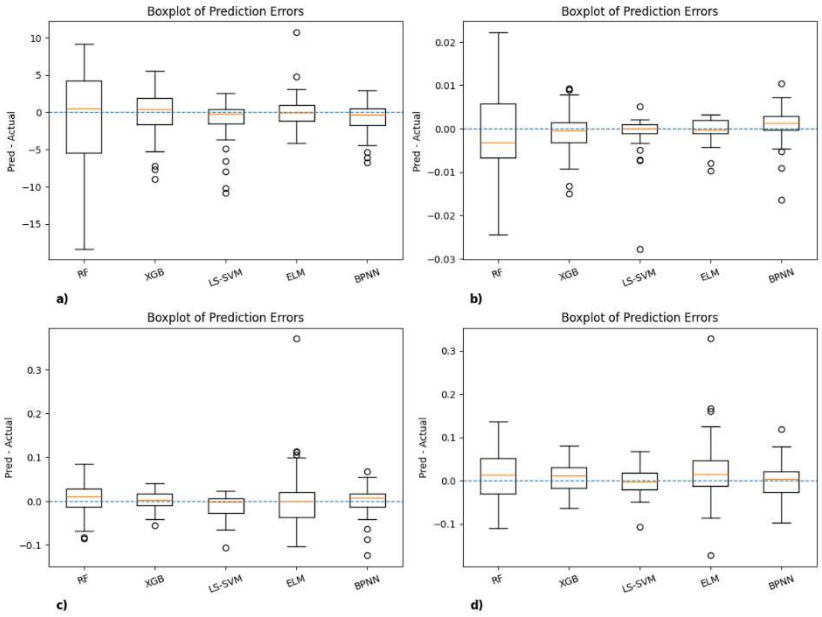


Figure 15: Boxplot representation of prediction errors (Predicted − Actual) for (a) Nu, (b) f, (c) η, and (d) N_s.

Based on the analysis of the boxplot, there are some outliers in all the models, especially in the values of *Nu* and N_s. Such deviations are normally linked with extreme conditions of inputs when the response behaviour is highly nonlinear. Though these few exceptions exist, most of the predictions fall within a small error margin. The fact that there are no vast groups of extreme more interesting the complexity of these responses.

On the whole, the error analysis indicates that the chosen model and specifically LS-SVM offers valid and objective predictions with low variability. The narrow error distributions, the centred residuals and the small number of outliers are indicators of high model robustness and the model can be used in practice in thermohydraulic applications.

6.9 Regression Error Characteristics

Regression Error Characteristic (REC) curves were used to offer a more detailed evaluation of the model performance than the traditional error measures. REC curves characterize the dependence between the error tolerance, and the resultant prediction coverage which is the fraction of samples whose absolute prediction error is within a given tolerance. The REC function can be mathematically written as:

$$F(\epsilon) = P(|y - \hat{y}| \leq \epsilon) \tag{26}$$

where y and $\hat{y}$ are the actual and predicted values, respectively. A steeper REC curve means that higher proportion of prediction attains low error and hence improved model performance.

REC curves were generated for all output variables (*Nu, f,* η, and N_s) using the testing dataset, while maintaining consistency in error tolerance scaling across models. A common ϵ grid was constructed based on the 98th percentile of pooled absolute errors to avoid distortion from extreme outliers. As shown in Figure 16, the curves exhibit a monotonic increase, indicating that prediction coverage improves as allowable error increases. For all outputs, advanced models reach high coverage values at relatively low error thresholds, demonstrating strong predictive capability. Overall, the REC-based evaluation confirms that LS-SVM provides the most reliable and robust predictions across all output variables. The consistency between REC trends, parity plots, and statistical metrics further strengthens the validity of the proposed modeling framework.

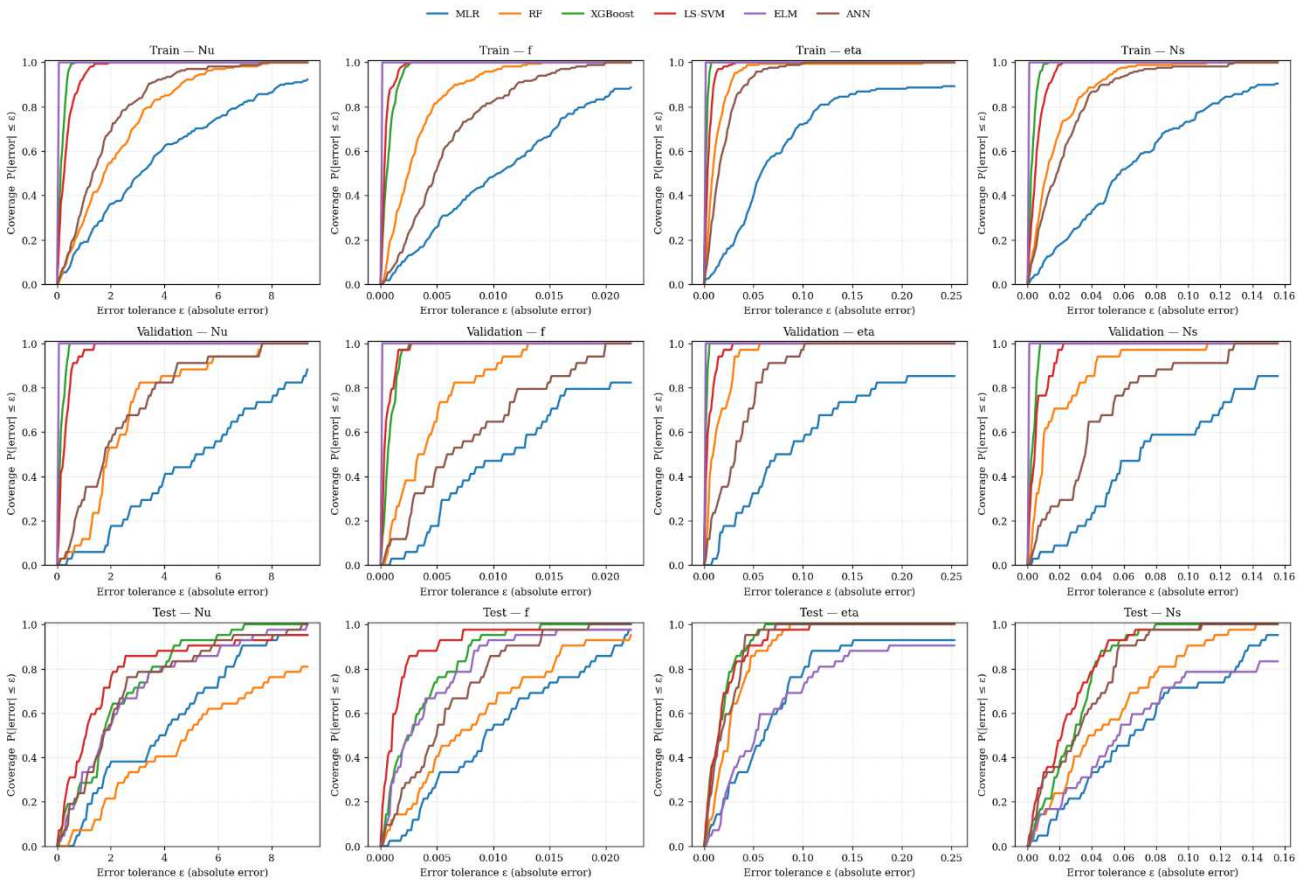


Figure 16: REC curves for training, validation, and testing datasets.

6.10 Explainable AI-Based Feature Contribution Analysis

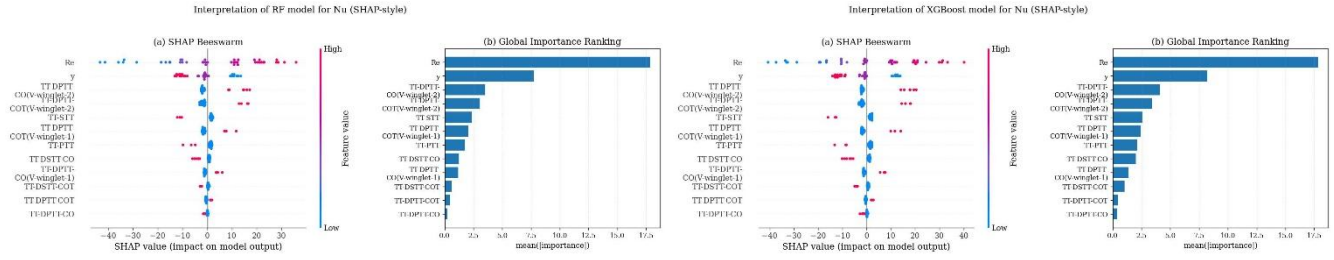
Although predictive accuracy offers quantitative confirmation of the model performance, it is imperative to comprehend the effect of each input parameters on the predictions to enable scientific interpretation and practical use. To do this, an explainable AI (XAI) system was implemented, integrating SHAP (SHapley Additive explanations) with treebased models and permutation-based importance with other learning models. The given hybrid approach helps to make sure that every model is interpreted through the method that is compatible with its internal structure, thus, preventing the bias of approximation, but preserving the consistency of features relevance analysis.

Figures 17(a) and (b) present the SHAP beeswarm plots and corresponding global importance rankings for RF and XGBoost models, respectively, for the prediction of Nusselt number (Nu). The results clearly indicate that Reynolds number (Re) is the most influential parameter, with higher values consistently contributing positively to the predicted heat transfer. This observation aligns well with established thermofluid principles, where increased flow intensity enhances convective heat transfer. The geometric parameter y also shows significant influence, although its impact varies depending on its magnitude, indicating nonlinear interaction

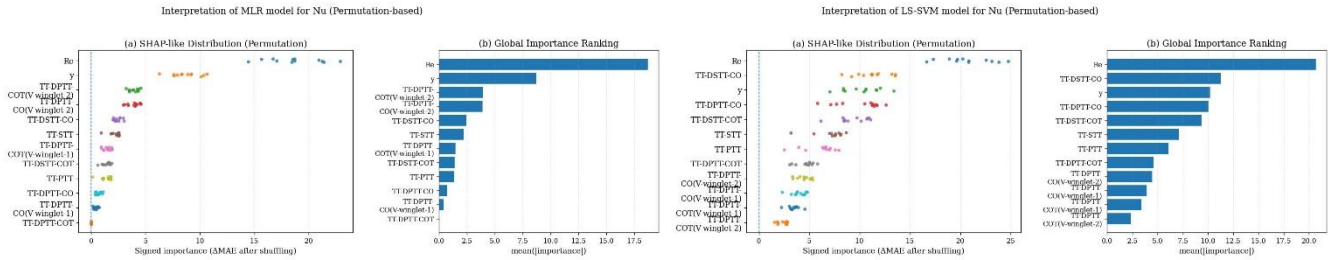
effects. Secondary features such as TT-DPTT, COT, and CO (associated with winglet configurations) contribute to refining the prediction, particularly in regions where flow behaviour becomes complex. The global importance rankings further confirm that Re and y dominate the prediction process, while other parameters provide incremental but necessary adjustments.

For models such as Multiple Linear Regression (MLR), LS-SVM, ELM, and ANN, permutation-based feature importance was adopted. Unlike SHAP, this approach is model-agnostic and evaluates feature relevance by measuring the increase in prediction error when a feature is randomly shuffled. Figures 17(c)–(f) illustrate the SHAP-like distribution of feature importance and corresponding global rankings obtained from permutation analysis. The results consistently show that Re remains the dominant feature across all models, reinforcing its fundamental role in governing heat transfer behaviour. However, compared to tree-based models, nonlinear models such as LS-SVM and ANN exhibit a more distributed importance structure, where interaction-based features (e.g., TT-DSTT- CO, TT-DPTT-CO) gain increased significance. In contrast, MLR demonstrates a simpler and more linear importance distribution, reflecting its limited capability in capturing complex relationships among variables.

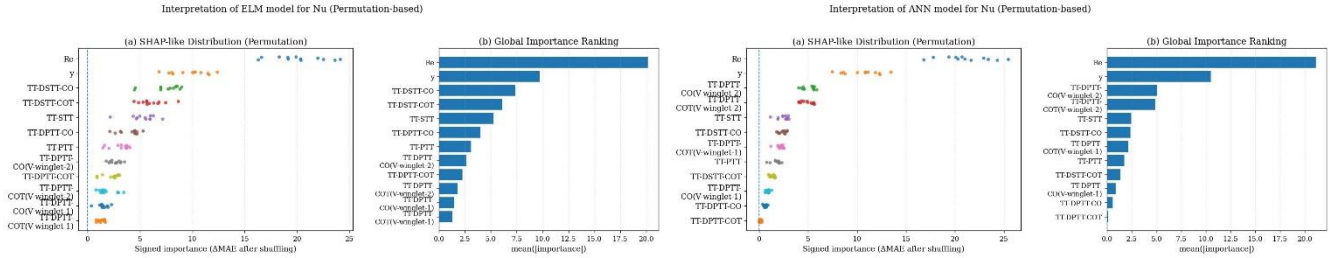
A consistent pattern emerges across all interpretation techniques: Reynolds number (Re) and geometric parameter (y) are the primary drivers of heat transfer performance. This agreement across different models and interpretation methods indicates that the identified feature importance is not model-dependent but inherent to the physical system. Tree-based models (RF and XGBoost) provide more stable and interpretable importance distributions, whereas kernel-based and neural models capture more complex feature interactions, albeit with slightly increased variability. Importantly, the consistency between SHAP-based and permutation-based interpretations strengthens the reliability of the explainability results and confirms that the proposed modeling framework captures physically meaningful relationships.



(a) RF (SHAP-based) (b) XGBoost (SHAP-based)



(c) MLR (Permutation-based) (d) LS-SVM (Permutation-based)



(e) ELM (Permutation-based) (f) ANN (Permutation-based)

Figure 17: Explainable AI analysis based feature contribution distributions and corresponding global importance rankings.

6.11 Optimization Analysis

To further investigate the real-life applicability of the created machine learning framework, a multi-objective optimization study was performed. The aim was to determine the best operating conditions, which would maximize the heat transfer performance and at the same time reduce the flow resistance and entropy generation. Surrogate predictors that were trained machine learning models were employed to assess the objective functions effectively.

1) Formulation of Multi-objective Optimization Problem: Multi-objective Optimization Problem was expressed by taking into account the conflicting character of thermo-hydraulic parameters. The aim was to maximize Nusselt number (Nu), thermal performance factor (η), and minimize the friction factor (f) and entropy generation number (N_s). This can be mathematically formulated as:

$$\text{Maximize} \quad \text{Nu}, \qquad \eta \tag{27}$$

$$\text{Minimize} \quad f, \qquad N_s \tag{28}$$

subject to:

$$Re_{min} \leq Re \leq Re_{max}, \qquad y_{min} \leq y \leq y_{max} \tag{29}$$

$$\text{TapeType} \in \text{STT, PTT, DPTT, etc.} \quad (30)$$

The machine learning models were embedded within the optimization framework, enabling rapid evaluation of candidate solutions without the need for repeated simulations or experiments.

2) Genetic Algorithm (GA) Optimization Results: A Genetic Algorithm (GA) was employed to explore the design space and identify optimal solutions. The process of optimization showed stable convergence, as the best fitness value increased rapidly at the beginning of the generations and then only slightly decreased. Referring to Table II, the findings reveal that the most efficient configuration is one that gives a high Reynolds number with a particular taping geometry (STT) that optimizes heat transfer without compromising friction and entropy to an acceptable level.

TABLE II: Optimal design variables and predicted outputs obtained from GA.

Parameter	Value
Reynolds number (Re)	21587.31
Pitch ratio (y)	2.0
Tape type	STT
Nu	124.10
f	0.1139
η	2.0352
N_s	0.8479

3) Trade-off Analysis Between Nu, f, η, and N_s: The outcome the optimization shows a clear trade-off of enhancement of heat transfer versus resistance to flow. With increasing Nusselt number, there are also tending to increase the friction factor because the turbulence effects and mixing effects also increase. In a similar manner, thermal gradients as well as viscous dissipation affect entropy generation. The Pareto-optimal solutions indicate that the increase in thermal performance factor (η) comes by sacrificing a little more friction losses. This action proves the fact that this is a multi-objective nature of the problem as no one solution can maximize all of the objectives at the same time.

4) Pareto-Optimal Design Solutions: The Figure 18 illustrates the Pareto front gained with the help of NSGA-II that helps understand the heat transfer enhancement rate is also reduced by friction factor. The Pareto front corresponds to each point of which the improvement in one objective will result in a compromise in the other. A small number of representative Pareto-optimal solutions are given in Table III to give a succinct representation of the good design configurations.

It is found out that higher values of *Nu* are associated with the higher friction factor and lowering the friction factor results in poor heat transfer performance. The Pareto front offers a range of the best solutions, which

can be chosen according to the demands of a particular design. The optimization of findings also shows that the STT configuration is always in optimal solutions, implying that it is effective in providing balanced thermo-hydraulic performance.

TABLE III: Representative Pareto-optimal solutions obtained from NSGA-II.

Re	y	Tape Type	Nu	f	η	N_s
10449	2.0	STT	72.93	0.1907	2.24	0.75
11714	2.0	STT	78.45	0.1788	2.20	0.76
12263	2.0	STT	80.87	0.1739	2.18	0.76

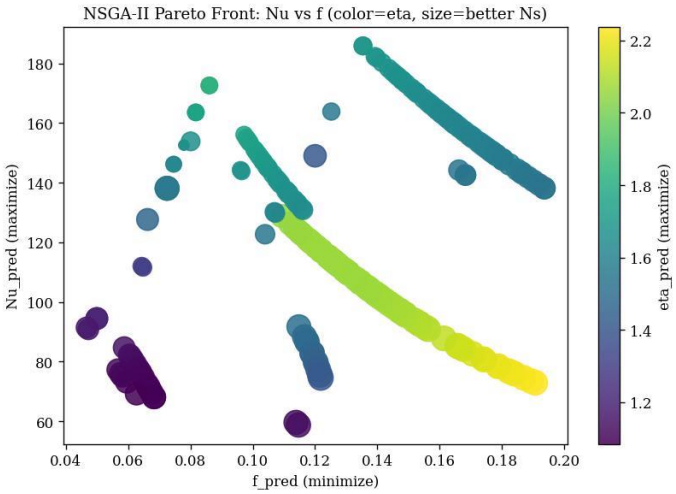


Figure 18: Pareto front obtained using NSGA-II showing trade-off between Nu and f (color represents η, marker size represents N_s)

6.12 Cross-Validation Analysis for Model Generalization

To evaluate the robustness and generalization capability of the developed models, a 5-fold cross-validation (CV) study was conducted. In this approach, the dataset was divided into five subsets, where each subset was used once as a testing set while the remaining subsets were used for training. The reported results represent the mean and standard deviation of performance metrics across all folds. Table IV summarizes the cross-validation performance of all models in terms of R^2, MAE, MSE, RMSE, and MAPE for each output variable. The inclusion of standard deviation provides insight into the stability of the models, where lower variation indicates more consistent performance across different data splits.

It can be observed that LS-SVM and XGBoost consistently achieve high R^2 values with relatively low standard deviations across all outputs, indicating strong predictive capability and stable generalization. In particular, LS-SVM demonstrates highly consistent performance for *Nu* and *f*, with minimal variability, highlighting its robustness. The ELM model shows excellent performance for Nu and f, achieving very high R^2 values; however, its performance significantly degrades for η and N_s, accompanied by higher standard deviations. This suggests that ELM may struggle to generalize for more complex and nonlinear responses. BPNN provides competitive results across most outputs but exhibits moderate variability, indicating sensitivity to data splits. Similarly, Random Forest shows relatively stable but lower performance compared to advanced models. Overall, the cross-validation analysis confirms that LS-SVM and XGBoost offer the best trade-off between accuracy and stability, while also highlighting the variability of certain models when applied to complex thermohydraulic responses such as entropy generation.

TABLE IV: 5-fold cross-validation results (mean ± standard deviation) for all models.

Model	Output	R^2	MAE	MSE	RMSE	MAPE (%)
RF	Nu	0.9249±0.0197	5.9472±0.4918	59.1583±14.9250	7.6477±0.9162	5.96±0.28
	f	0.9237±0.0321	0.0079±0.0010	0.0001±0.0000	0.0106±0.0006	6.93±154
	η	0.9495±0.0369	0.0337±0.0098	0.0029±0.0034	0.0489±0.0261	2.37±0.48
	N_s	0.8717±0.0465	0.0423±0.0054	0.0030±0.0007	0.0544±0.0066	4.04±0.40
XGBoost	Nu	0.9821±0.0170	2.4841±0.6352	14.3458±13.499	3.5292±1.5374	2.42±0.56
	f	0.9810±0.0063	0.0035±0.0006	0.0000±0.0000	0.0054±0.0006	3.01±0.85
	η	0.9811±0.0104	0.0201±0.0052	0.0010±0.0010	0.0301±0.0134	1.46±0.30
	N_s	0.9408±0.0127	0.0280±0.0046	0.0014±0.0003	0.0375±0.0033	2.69±0.42
LS-SVM	Nu	0.9899±0.0028	1.7813±0.1605	8.0271±2.0456	2.8124±0.3829	1.58±0.13
	f	0.9857±0.0069	0.0026±0.0005	0.0000±0.0000	0.0047±0.0014	1.92±0.26
	η	0.9760±0.0195	0.0211±0.0069	0.0014±0.0017	0.0331±0.0196	1.46±0.38
	N_s	0.9445±0.0198	0.0273±0.0040	0.0013±0.0004	0.0360±0.0060	2.63±0.42
ELM	Nu	0.9940±0.0015	1.5018±0.2587	4.9076±1.8003	2.1842±0.4133	1.62±0.40
	f	0.9888±0.0124	0.0025±0.0007	0.0000±0.0000	0.0037±0.0015	2.25±0.86
	η	0.8969±0.0477	0.0461±0.0064	0.0047±0.0018	0.0677±0.0147	3.33±0.48
	N_s	0.6976±0.1086	0.0593±0.0116	0.0073±0.0029	0.0840±0.0175	5.83±136
BPNN	Nu	0.9765±0.0124	2.7634±0.6545	17.4589±7.1120	4.1009±0.8955	2.84±0.62
	f	0.9429±0.0215	0.0053±0.0010	0.0001±0.0000	0.0093±0.0018	4.94±0.92
	η	0.9487±0.0083	0.0324±0.0045	0.0024±0.0007	0.0490±0.0066	2.36±0.33
	N_s	0.7780±0.0557	0.0506±0.0080	0.0054±0.0017	0.0727±0.0118	4.94±0.74

7. Conclusions

The key outcomes of the present investigation are summarized as follows:

- The Nusselt number (Nu) associated with twisted tape inserts exhibits an inverse relationship with the twist ratio, increasing as the twist ratio decreases. Moreover, the heat transfer augmentation for the modified twisted tape configurations follows a progressive ascending order: STT < PTT < DSTT-CO < DSTT-COT < DPTT-CO < DPTT-COT < DPTT-CO (V-winglet-1) < DPTT-COT (V-winglet-1) < DPTT-CO (V-winglet-2) < DPTT-COT (V-winglet-2).
- The DPTT-COT (y = 6) insert configuration exhibits the lowest frictional losses among all the geometries considered. The DPTT-COT (V-winglet-2, y = 4) configuration attains the maximum thermal performance factor (η), with a value of 1.82. The lowest entropy generation number (N_s) is observed for the DPTT-COT configuration with V-winglet-1 at a twist ratio of y = 6.
- The proposed ML framework successfully integrates predictive modelling, explainable AI, and multi-objective optimization for thermo-hydraulic analysis. Among all models, LS-SVM and XGBoost consistently achieved higher accuracy, stability, and better generalization performance. The inclusion of SHAP-based interpretation and Pareto optimization enhances both physical insight and practical applicability. Overall, the study provides a reliable and efficient approach for designing optimized thermo-hydraulic systems.

References

1. Eiamsa-ard S, Thianpong C, Promvonge P. Experimental investigation of heat transfer and flow friction in a circular tube fitted with regularly spaced twisted tape elements. Int. Communication in Heat Mass Transfer. 2006; 33:1225–33.
2. Promvonge P. Thermal augmentation in circular tube with twisted tape and wire coil turbulators. Energy Conversion and Management. 2008;49:2949-55.
3. Thianpong C, Eiamsa-ard P, Wongcharee K, Eiamsa-ard S. Compound heat transfer enhancement of a dimpled tube with a twisted tape swirl generator. International Communications in Heat and Mass Transfer. 2009;36:698–704.
4. Eiamsa-ard S, Seemawute P, Wongcharee K. Influences of Peripherally cut twisted tape insert on heat transfer and thermal performance characteristics in laminar and turbulent tube flows. Experimental Thermal and Fluid Science. 2010;34:711–19.
5. Eiamsa-ard S, Thianpong C, Eiamsa-ard P. Turbulent heat transfer enhancement by counter/co-swirling flow in a tube fitted with twin twisted tapes. Experimental Thermal and Fluid Science. 2010;34:53 – 62.

6. Bhuiya MMK, Chowdhury MSU, Shahabuddin M, Saha M, Memon LA. Thermal characteristics in a heat exchanger tube fitted with triple twisted tape inserts. International Communications in Heat and Mass Transfer. 2013;48:124–32.
7. Vashistha C, Patil AK, Kumar M. Experimental investigation of heat transfer and pressure drop in a circular tube with multiple inserts. Applied Thermal Engineering. 2016;96:117–29.
8. Piriyarungrod N, Kumar M, Thianpong C, Pimsarn M, Chuwattanakul V, Eiamsa-ard S. Intensification of thermo-hydraulic performance in heat exchanger tube inserted with multiple twisted-tapes. Applied Thermal Engineering. 2018;136:516-30.
9. Eiamsa-ard S, Changcharoen W, Beigzadeh R, Eiamsa-ard P, Wongcharee K, Chuwattanakul V. Influence of co/counter arrangements of multiple twisted-tape bundles on heat transfer intensification. Chemical Engineering and Processing - Process Intensification. 2021;160:108304.
10. Ahamed JU, Wazed MA, Ahmed S, Nukman Y, Ya TMYST, Sarkar MAR. Enhancement and Prediction of Heat Transfer Rate in Turbulent Flow Through Tube With Perforated Twisted Tape Inserts: A New Correlation. ASME. J. Heat Transfer. 2011;133(4):041903.
11. Bhuiya MMK, Chowdhury MSU, Saha M, Islam MT. Heat transfer and friction factor characteristics in turbulent flow through a tube fitted with perforated twisted tape inserts. International Communications in Heat and Mass Transfer. 2013;46:49–57.
12. Bhuiya MMK, Azad AK, Chowdhury MSU, Saha M. Heat transfer augmentation in a circular tube with perforated double counter twisted tape inserts. International Communications in Heat and Mass Transfer. 2016;74:28-26.
13. Kumar B, Kumar M, Patil AK, Jain S. Effect of V cut in perforated twisted tape insert on heat transfer and fluid flow behavior of tube flow: An experimental study. Experimental Heat Transfer. 2019;32(6):524-44.
14. Kumar B, Patil AK, Jain S, Kumar M. Study of Entropy Generation in Heat Exchanger Tube with Multiple V Cuts in Perforated Twisted Tape Insert: ASME. Journal of Heat Transfer. 2019;141:081801-1.
15. Jayranaiwachiraa N, Promvongea P, Thianponga C, Skullong S. Entropy generation and thermal performance of tubular heat exchanger fitted with louvered corner-curved V-baffles. International Journal of Heat and Mass Transfer. 2023;201(1):123638.
16. Heeraman J, Sandeep C, Chaurasiya PK. Heat transfer enhancement in double pipe heat exchanger: exploring twisted tape inserts with dimple configuration. *J Therm Anal Calorim*. 2024;149:8839–56.
17. Mertaslan OM, Keklikcioglu O. Investigating heat exchanger tube performance: second law efficiency analysis of a novel combination of two heat transfer enhancement techniques. *J Therm Anal Calorim*. 2024. https://doi.org/10.1007/s10973-023-12842-6.
18. Celik N, Pusat G, Tasar B, Kapan S, Kistak C. Machine learning regression analysis of a heat exchanger with corrugated tape turbulators, by means of second law analysis. Thermal Science and Engineering Progress. 2025;66:104033.
19. Khan MZA, Khan HA, Aziz M. Performance optimization of heat-exchanger with delta-wing tape inserts using machine learning. *Applied Thermal Engineering*. 2022;216: 119135.
20. Kunakote T, Promthaisong P, Kumar S, Bubphachot B, Chompookham T, Siriwan N, Sabangban N, Wansasueb K. Comparative analysis of machine learning-assisted metaheuristic optimization algorithms for corrugated tube heat exchanger design. Results in Engineering. 2026;29: 108785.
21. Han H, Yu R, Li B, Zhang Y. Multi-objective optimization of corrugated tube inserted with multi-channel twisted tape using RSM and NSGA-II. Applied Thermal Engineering. 2019;159: 113731.
22. Cengel Y, Ghajar A. Heat and Mass Transfer - Fundamentals and Applications. 5th Edition. McGraw-Hill. New York. NY. 2014.

23. Zimparov VD, Vulchanov NL, Performance Evaluation Criteria for Enhanced Heat Transfer Surfaces. Int. J. Heat Mass. Transf. 1994;37(12):1807–16.
24. Qi C, Wang G, Yan Y, Mei S, Luo T. Effect of Rotating Twisted Tape on Thermo-Hydraulic Performance of Nano-fluids in Heat-Exchanger Systems. Energy Convers. Manage. 2018;166:744−57.